Synthesis and spectroscopic characterisation of $LiFePO_4$ cathode materials

Z. LAZAREVIĆ[a,*], G. KRIŽAN[b,c], J. KRIŽAN[d], M. MITRIĆ[e], N. PAUNOVIĆ[a], A. MILUTINOVIĆ[a], N. ROMČEVIĆ[a]
[a]*Institute of Physics, University of Belgrade, Pregrevica 118, 11080 Belgrade, Serbia*
[b]*Department of Materials Chemistry, National Institute of Chemistry, Ljubljana, Slovenia*
[c]*Faculty of Chemistry and Chemical Technology, University of Ljubljana, Ljubljana, Slovenia*
[d]*AMI d.o.o., Trstenjakova ulica 5, Ptuj, Slovenia*
[e]*Institute of Nuclear Sciences Vinča, University of Belgrade, Belgrade, Serbia*

Lithium iron phosphate ($LiFePO_4$) are synthesized in complete and incomplete combustion and calcined at 700°C. The obtained samples were characterized by XRD, IR spectroscopy and magnetic measurement. Morphology of samples was controlled by SEM. The aim of this work is to show that it is possible to achieve a desired crystal phase by pulse combustion in a relatively cheap and fast way. The extremely rapid synthesis of almost pure phase material is possible due to the reduction in size of interacting particles and to an enormous number of collisions between them as a result of the strong turbulent flow associated with explosive combustion.

(Received January 13, 2018; accepted April 8, 2019)

Keywords: Lithium iron phosphate, IR spectroscopy, Magnetic measurements

1. Introduction

Many researchers worked in developing the rechargeable lithium battery. Synthesis of new cathode materials for high capacity rechargeable lithium ion batteries is experiencing a great expansion in past few decades [1]. Chemistry, performance, cost and safety characteristics vary across battery types. $LiFePO_4$ crystallizes in the orthorhombic system (No. 62) with *Pnma* space group. It consists of a distorted hexagonal-close-packed (hcp) oxygen network forming 16 octahedral and 32 tetrahedral sites. There are two distinct and differ in size octahedral sites in this material: M1 is occupied by Li^+, and M2 is occupied by Fe^{2+}. The M1 sites form linear chains of edge sharing octahedra along the *b*-axis within Li^+ can be transferred to the anode in the first charge process, compensating for the oxidation of iron (Fe^{2+} to Fe^{3+}) [2]. The structure may contain one lithium ion per formula unit, which results in the theoretical capacity of 170 $mAhg^{-1}$. However, these one-dimensional paths are particularly vulnerable to blockage by defects and impurities. The M2 sites form zigzag lines of corner sharing octahedra and there is no continuous network of FeO_6 edge-shared octahedra that might contribute to electronic conductivity [3, 4]. Cations, Li (M1) and Fe (M2), are placed in half the octahedral sites and P ions in one-eighth of the tetrahedral sites [5]. The peculiar distribution of Li^+ and Fe^{2+} within the octahedral sites generates layers that have a direct impact on both electronic and ionic conductivities. Corner-shared FeO_6 octahedra are linked together in the *bc*-plane [6]. The FeO_6 octahedra are distorted lowering their local cubic-octahedral O_h to the C_s symmetry. The tetrahedral PO_4 polyanions bridge neighbouring layers of FeO_6 octahedra by sharing a common edge with one FeO_6 octahedron and two edges with LiO_6 octahedra. The PO_4 bridges provide three-dimensionality to the lattice and structure stability. Low intrinsic electrical conductivity and low Li-ion diffusion can be override by reducing the size of LFP nano-crystallites (and the diffusion path length for electrons and Li^+ ions), and by making composites with conductive graphitic materials, what resulting in better electronic contact between the particles.

It is generally known that there are a number of methods for obtaining Li-ion cathode materials. In the case of $LiFePO_4$ these methods can be divided into two groups - solid state syntheses and solution syntheses [7]. Solid state techniques are carried out at high temperatures without the addition of any solvent. On the other hand, solution based methods are based on reactions that take place in the presence of appropriate solvent systems.

There are some excellent reviews on the properties of $LiFePO_4$ that deal with its structural, morphological, electrochemical, and other physical properties targeting its cathode application. In a review paper [2] provides a detailed overview of the synthetic methods with the possible advantages and disadvantages of obtaining $LiFePO_4$ powders. A major difficulty related to the synthesis of orthophosphate $LiFePO_4$ comes from the existence, of two oxidation degrees of iron in nature, namely Fe^{2+} and Fe^{3+}, which makes the preparation of this material difficult.

Solid state synthesis, mechano-chemical activation, carbothermal reduction and microwave heating are based on solid state chemistry and are the most common solid-state methods for preparing $LiFePO_4$ powders [2, 8, 9].

Solid state methods are of importance in terms of obtaining ordered crystal structure in a simple way at elevated temperatures.

Although solid state methods are simple to use, they are typically time and energy consuming techniques and often lead to large particle size, low purity and deliver relatively poor electrochemical performance. Therefore, solution-based methods are of increasing importance as they often result in smaller and more uniform particle sizes, higher purity, more homogeneous carbon coating and higher electrochemical capacity. Hydrothermal synthesis [10], sol-gel synthesis [11], spray pyrolysis [12], co-precipitation [13] and micro emulsion drying [14] are common solution-based methods used for the preparation of $LiFePO_4$ powders.

An interesting technique is also the solution combustion synthesis, utilizing a reaction between metal nitrates an organic fuel, intricately mixed in a solution, after the solvent is evaporated [6, 15]. The method is easy to scale, very energy efficient, can combust stoichiometric fuel and air mixtures and is suitable for the production of powders in nanometric range because of acoustically driven droplet size reduction [16]. Furthermore, this method is very fast as the heat transfer is enhanced in the acoustic field of pulse combustion and solution combustion synthesis proceeds in a fraction of a second once the components reach the decomposition temperature [15]. There is also no waste water since it evaporates and the only by products are flue gases common for burning carbonaceous fuels.

The main goal of our work was to produce $LiFePO_4$ by a pulse combustion reactor method. The obtained olivine $LiFePO_4$ was characterized using XRD, IR spectroscopy and magnetic measurement. The morphology was studied using scanning electron microscopy.

2. Experimental procedure

The investigated samples are produced in reactor with a Helmholtz-type pulse combustor. The reactor, its capabilities and operating conditions, as well as the control of the synthesis processes, are described comprehensively in Ref.-s [7, 17].

The precursor is sprayed with a two fluid nozzle, the spraying gas being 99.9 % nitrogen with a pressure of 1.5 bar and a flow of 45 NL min^{-1}, measured using a thermal mass flow-meter. The precursor composition is 41,3 g of $LiNO_3$, 230,5 g of $Fe(NO_3)_3.9H_2O$, 69,0 g of $NH_4H_2PO_4$, 137,1 g of urea, 78,2 g of sucrose and 46,4 g of NH_4NO_3, dissolved in 700 g of deionized water. The reactor is operating under different conditions with the main difference being the frequency and amplitude of pressure oscillations. The sample was synthesized in reductive reactor conditions with low pressure amplitude (10 mbar). Obtained material was annealed in the inert atmosphere. Annealing is taking place in an electrical oven under a constant argon flow and in presence of carbon at 700 °C for 6 h. High temperature and inert environment allow a reduction of Fe^{3+} from α-Fe_2O_3 and formation of additional $LiFePO_4$ according to: $4\ Li_3Fe_2(PO_4)_3 + 2\ Fe_2O_3 + 3C \rightarrow 12\ LiFePO_4 + 3CO_2$.

Four types of samples were investigated: 1) samples of the *as prepared* material synthesized in complete combustion and resonance mode of reactor (CC); 2) annealed samples of the material synthesized in complete combustion (A-CC); 3) samples of the *as prepared* material synthesized in incomplete combustion and resonance mode of reactor (ICC) and 4) annealed samples of the material synthesized in incomplete combustion (A-ICC).

Characterization of the sample was carried out by several methods:

• X-ray diffraction analysis was performed on X-ray diffractometer (Rigaku Corporation, Japan) at room temperature. CuKα radiation (λ = 0.15418 nm) with a step size of 0.02° in the range of 2θ = 15-60° was used for all samples. The peaks were identified using the Powder Diffraction File (PDF) database created by International Centre for Diffraction Data (ICDD).

• The infrared (IR) measurements were carried out with a BOMMEM DA-8 FIR spectrometer. A DTGS pyroelectric detector was used to cover the wave number range from 50 cm^{-1} to 700 cm^{-1}.

• Magnetic susceptibility measurements were carried out at Cryogenic vibrating sample magnetometer (VSM) with an ultra-sensitive superconducting quantum interference device (SQUID) in the temperature range 4-160 K. *AC* magnetic susceptibility were performed using a mutual inductance method with an alternate excitation field of 5 Oe and frequencies in the range 7-10000 Hz.

• Scanning electron microscopy - SEM (Zeiss Supra 35 VR) was used to make images of the particles.

3. Results and discussion

X-ray diffraction analysis was used to identify the crystalline phases of the investigated samples. Fig. 1 shows the XRD patterns of two as prepared samples (CC and ICC) and two annealed samples (A-CC and A-ICC). Spectra of samples CC and ICC are with subtracted baselines. Original diffraction patterns are shown in inserts.

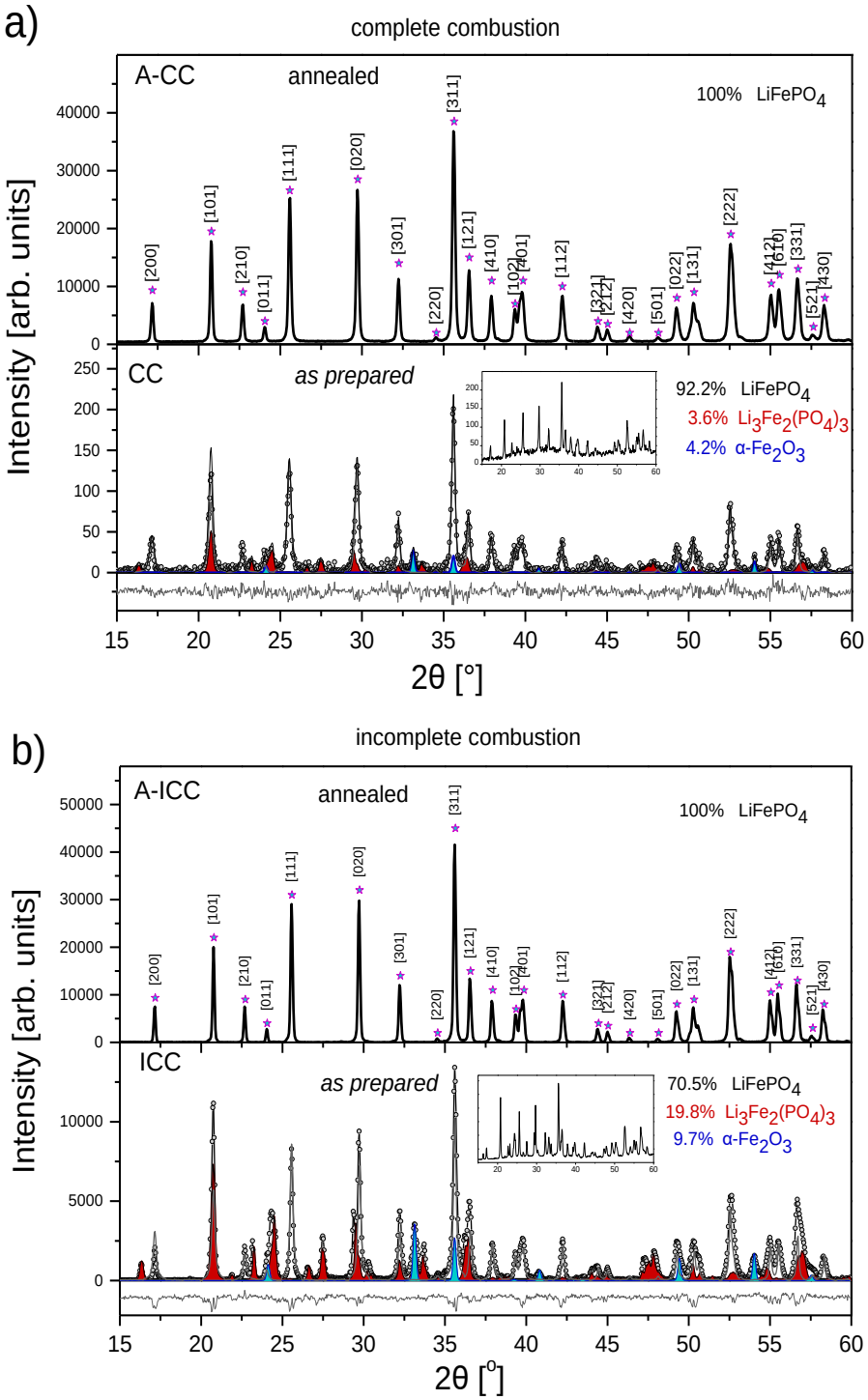

Fig. 1. a) XRD spectra of samples obtained by complete combustion: as prepared CC and annealed A-CC; b) XRD spectra of samples obtained by incomplete combustion: as prepared ICC and annealed A-ICC

All diffraction patterns were analysed by Rietveld refinement software. Except dominant $LiFePO_4$ phase, *as prepared* samples contain phases with Fe^{3+}: α-$Li_3Fe_2(PO_4)_3$ and α-Fe_2O_3. Phase content is given in Fig. 1. A sample CC, of the material obtained in complete combustion has over 92% of $LiFePO_4$ phase and sample ICC obtained in incomplete combustion has 70.5%. After annealing at 700 °C for 6 h in reductive atmosphere both materials exhibit pure olivine $LiFePO_4$ phase.

Annealing of *as prepared* material leads to certain enlargement of $LiFePO_4$ crystallographic cell volume. In A-CC sample enlargement is 0.01% related to CC sample (crystal cell constant *a* increases 0.07%; *b* increases 0.03%; *c* decreases 0.01%) and internal strain decreases for 28%. In A-ICC sample enlargement is even 0.3% related to ICC sample (crystal cell constant *a* increases 0.1%; *b* increases 0.2%; *c* slightly decreases 0.02%) but internal strain increases for 5%. The results of Rietveld

refinement are given in Table 1 for the fraction of pure LFP-phase in the investigated samples.

Table 1. Fraction of pure LFP-phase in the investigated samples and the microstructural characteristics: crystal cell constants, crystallite size and strain obtained from the Rietveld analysis

Sample	Crystal cells constants [Å]			Size [nm]	Strain 10^{-4}
	a	*b*	*c*		
A-CC	10.3211	6.0039	4.6908	57.0	13.7
A-ICC	10.3228	6.0084	4.6897	71.3	13.2
CC	10.3140	6.0022	4.6912	30.3	19.08
ICC	10.3129	5.9956	4.6907	46.7	12.56

Similar behaviour is noticed for many nanocrystalline samples. Smaller nanoparticles with greater surfaces and more incomplete bonds have a great deal of $Li_{1-x}(Fe^{3+}, Fe^{2+})(PO_4)$ phase. $LiFePO_4$ and $FePO_4$ present both the *Pnma* olivine structure. Chemical extraction of Li^+ from $LiFe^{2+}PO_4$ results in oxidation of Fe^{2+} into Fe^{3+}. Decrease of ionic radii of Fe cation in crystallographic site M2 (4*c*) leads to changes in lattice parameters in $Fe^{3+}PO_4$.

According to Rousse at al. [18] in $FePO_4$, related to $LiFePO_4$, contractions of lattice along the *a* and *b* axis are -5.6% and -4.3%, respectively, and the *c* lattice parameter being increased by +1.5%. Gibot *at al.* [19] by *in situ* XRD analysis have registered a continuous shift of the diffraction peaks (and unit cell volume) during the charge/discharge of their $LiFePO_4$ cathode. This is equivalent to a continuous change of *x* in $Li_{1-x}(Fe^{3+}, Fe^{2+})(PO_4)$ material. In full discharged state, according to XRD, cathode material exhibits the smallest cell volume of 273 $Å^3$, close to those of the fully delithiated $FePO_4$ phase.

Our annealed samples have crystal cell volumes a little lower than LFP cell standard PDF card No. 81-1173 (a = 1.0330 nm, b = 0.6010 nm, and c = 0.4692 nm), or in Ref. [20] (a = 10.3131 Å, b = 6.0025 Å and c = 4.6948 Å). In light of Results in Table 1 all our samples contain a certain amount of delithiated $LiFePO_4$ and the amount of this phase is larger in *as prepared* samples.

The infrared reflectivity of all samples is rather low, only about 0.2. The highest values of 0.3 achieve peaks of annealed samples owing to better crystallinity. Spectra of annealed samples are very similar. General appearance of un-annealed samples spectra is different. Experimental spectra are properly fitted with 18 phonon modes. It is obvious that the concentration of electrons is small enough that there was no need for fitting of plasma frequency in the investigated range of spectra.

Kramers-Krönig (KK) analysis of reflectivity spectra gives $\varepsilon_2(\omega)$ and energy loss function, $\sigma(\omega) = \mathrm{Im}(-1/\varepsilon(\omega))$. Local maximums of $\varepsilon_2(\omega)$ correspond to the values of ω_{TO}, and local maximums of $\sigma(\omega)$ to ω_{LO}. Values of $\omega_{LO(TO)}$ obtained by fitting procedure are in accordance with values calculated by KK analysis (except the beginnings of spectra that were not fitted precisely owing to high level of noise). In Fig. 2 are given $\varepsilon_2(\omega)$ functions obtained from KK analysis for all investigated samples. Dotted "vertical" lines show modes with frequencies shifted in relation to the corresponding modes in the annealed samples. Full vertical lines show modes that stayed unchanged. In near normal incidence measurements TO modes correspond to minimums of transmittance. Only TO modes are IR active.

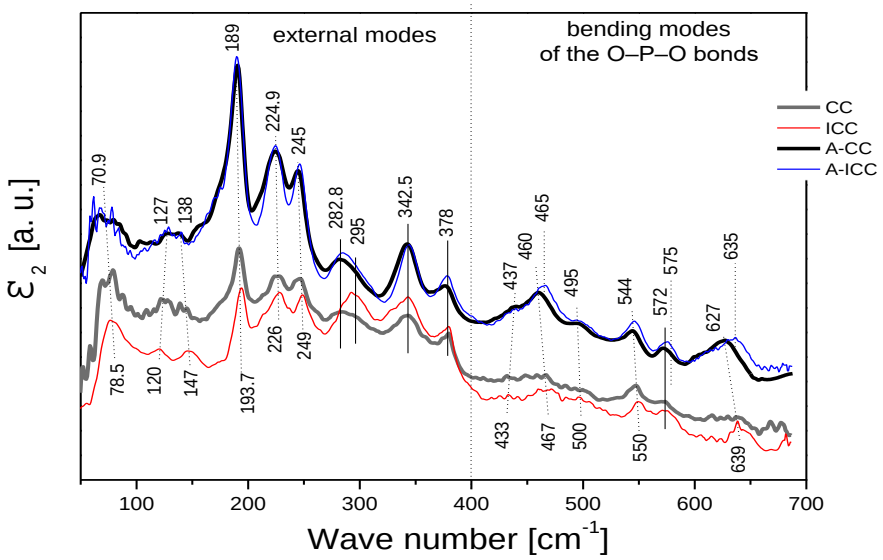

Fig. 2. Kramers-Krönig analysis of reflectivity spectra

Strength of TO modes, i.e. LO modes, can be deduced through fitting of reflectance spectra. Therefore, we can compare our $\varepsilon_2(\omega)$ functions with theoretical predictions of Shi [21] and available transmission/absorption measurements [22-27]. It should be bare in mind that intensity of peaks in $\varepsilon_2(\omega)$ doesn't correspond to real strength of modes obtained by fitting procedure.

The origin of a few coarse features at low wave numbers is not clear. We suppose that it can be a combination of acoustic modes activated by disorder. Further 15 phonons with remarkably reduced damping are attributed to optical modes of the crystal structure. Infrared reflectivity spectra of annealed samples A-CC and A-ICC evidently exhibit modes of $LiFePO_4$. Phonons with frequencies at 189, 224.9, 245 and 282.8 cm^{-1} are connected with vibrations of LiO_6 octahedrons. Peak at about 225 cm^{-1} is distinguishing for LiO_6 and related to asymmetric stretching vibration of Li - O bonds. Phonons at 324.5 and 378 cm^{-1} are connected with FeO_6 octahedrons and all together belong to external modes. From 400 to 647 cm^{-1} is the range of internal PO_4^{3+} anion bending modes. A weak mode at 437 cm^{-1} is probably a $B_{2u}(6)$ mode [26]. Modes of PO_4 at 460-495 in A-CC sample, and 465-495 in A-ICC sample, represent "ν_2" modes, *i.e.* symmetric O-P-O bending modes. ν_2 modes in LFP are a mixture of Li translations and PO_4 bending motions of the same symmetry. Burba and Frech [22] suggest that these bands in $LiFePO_4$ are predominantly Li-ion "cage modes", *ie.* Li-translation. At 572-627 cm^{-1} in A-CC and 575-635 cm^{-1} in A-ICC are ν_4 modes, *i.e.* anti-symmetric O-P-O bending modes.

By comparing literature data it can be seen that obtained values for certain mode vary a litle. Possible resons are different methods of producing samples, or different size of crystallites. For example, Burba and Frech were registered the doublet ν_2 at 470-506 cm^{-1}, in Ref.[22] at 465-503 cm^{-1}, or in Ref. [26] at 469-499 cm^{-1}. The positions of the other modes vary in similar way.

Since external modes of annealed samples do not differ from each other, the difference in values of internal modes could not be asscribed to the producing of samples. A blue shift of A-ICC internal modes could be explained by superposition of LFP modes and modes of slightly delithiated phase $Li_{1-x}(Fe^{3+}, Fe^{2+})PO_4$, or a small amount of $FePO_4$ – phase with olivine structure "invisible" for XRD.

Samples CC and ICC have broader modes with partially changed energies due to superposition of $LiFePO_4$ modes and modes of other phases Fe_2O_3 and $Li_3Fe_2(PO_4)_3$, registered by XRD analysis. Except modes from the group of FeO_6 vibrations (and two weak modes at the beginning of spectra), other modes are shifted toward higher frequencies. That can be explained by contraction of bonds in LiO_6 octahedral, as well as in PO_4 tetrahedral. Cell volume shrinking was observed by XRD analysis of *as prepared* samples. IR spectra suggest that for volume shrinking two reasons exists: presence of smaller Fe^{3+} cations in crystal cell and a lack of Li related to pure LFP phase. Contraction in LiO_6 suggest that phase without Li (like hematite), or delithiated phase is present together with LFP phase. In the range of 200-400 cm^{-1} a certain increasement of peaks intensity is noticeable especially in the case of ICC sample. This range corresponds to the strongest modes of $Li_3Fe_2(PO_4)_3$ phase [24]. Such behaviour confirms that ICC sample contains much more fraction of $Li_3Fe_2(PO_4)_3$ phase than CC sample.

AC-magnetic susceptibility measurements were shown that the sample of annealed A-CC material has a typical triphylite antiferromagnetic behaviour with a Neel temperature at 53.4 K [25, 27]. The sample A-ICC except the predominant triphylite transition has a visible AFM transition of delithiated $FePO_4$ phase at T_N = 130 K [25]. The results for poly-phase *as prepared* CC and ICC samples with small crystallites are shown in Fig. 3. Nell temperature of 29 K corresponds to $Li_3Fe_2(PO_4)_3$ phase [27] and about 51 K is a poorly visible antiferromagnetic transition of $LiFePO_4$. It means that *as prepared* samples are mostly superparamagnetic.

A peak at about 7.6 K in CC-sample (and 8.7 K in ICC) shifts toward higher temperatures with increasing measurement frequency. Such frequency dependence is specific for a spin glass. Therefore, a peak temperature is a spin-glass freezing temperature T_f [28]. The dependence of T_f with frequency is illustrated in the inset of Fig. 3.

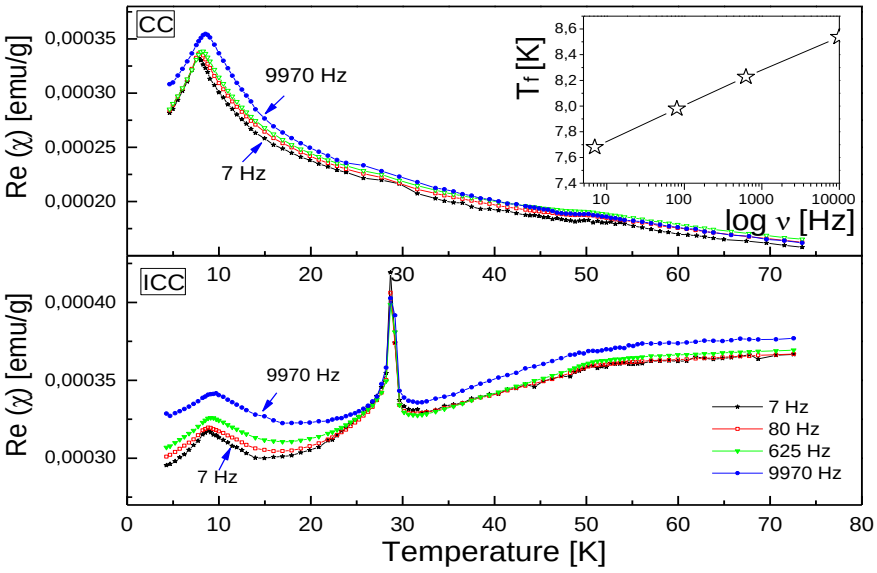

Fig. 3. AC susceptibility measurements at alternating fields with intensity 5 Oe and frequencies of 7, 80, 625 and 9970 Hz

SEM images of samples obtained by complete combustion (as prepared CC and annealed A-CC) and incomplete combustion (as prepared ICC and annealed A-ICC) are presented in Fig. 4. The difference in particle size is evident from images. The agglomerates are of approximately the same size (from 4 to 10μm), shaped like porous balls. In the annealed sample A-ICC are visible much larger structures than in A-CC sample. An average diameter of hollow spheres is about 10 μm. In the SEM image of the as prepared ICC sample (at the bottom, right) except globular form, a disk- like aggregates are seen. It can be seen a number of small shinny nanocrystals with average size about 30 nm. This supports the claim that particle size might affect the cell parameters, as indicating from Ritveld refinement of XRD data.

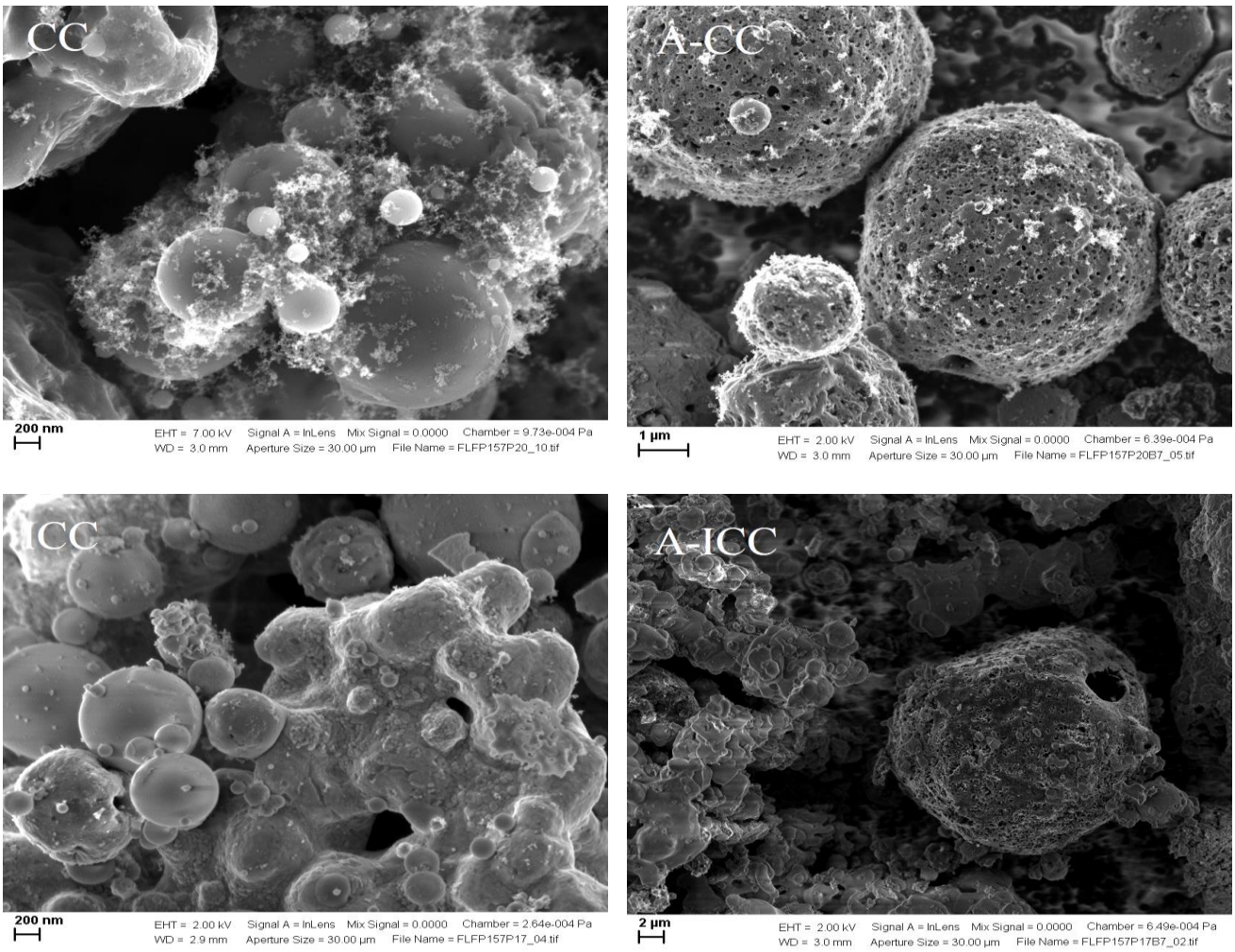

Fig. 4. SEM images of samples obtained by complete combustion (as prepared CC and annealed A-CC) and incomplete combustion (as prepared ICC and annealed A-ICC)

4. Conclusions

In this paper were investigated carbon coated $LiFePO_4$ cathode materials obtained by pulse combustion at the same temperature 700 °C, but in one case - under the conditions that leaded to complete combustion, and in the other case - under the conditions of incomplete combustion. After XRD analysis it seemed that in both cases after annealing we have obtained a good cathode material (samples A-CC and A-ICC). Therefore, further analysis IR and magnetic measurement, were implied that these, at first sight, perfect samples differed from each other. Analysis showed a significant excess of Fe^{3+} ions in the A-ICC sample and the magnetic measurements definitively identified a small quantity of delithiated $FePO_4$ phase in these sample.

In conclusion, performed measurements and analyses proved that (among investigated samples) the sample obtained under the applied conditions of complete combustion and annealed after that (in the presence of carbon under a constant argon flow at 700 °C for 6 hours),

A-CC, has a good structure and morphology that promises good electrochemical properties.

Acknowledgements

This work was financially supported by the Ministry of Education, Science and Technological Development of the Republic of Serbia through Project No. III 45003. The authors would like to thank Dr Izabela Kuryliszyn-Kudelska from Institute of Physics, Polish Academy of Science for assistance of magnetic measurements.

References

[1] T. V. S. L. Satyavani, A. Srinivas Kumar, P. S. V. Subba Rao, Engineering Science and Technology, an International Journal **19**, 178 (2016).
[2] D. Jugović, D. Uskoković, J. Power Sources **190**, 538 (2009).
[3] D. Morgan, A. Van der Ven, G. Ceder, Electrochem. Solid St. **7**(2), A30 (2004).
[4] S. Okada, S. Sawa, M. Egashira, J. Yamaki, M. Tabuchi, H. Kageyama, T. Konishi, A. Yoshino, J. Power Sources **97-98**, 430 (2001).
[5] K. Zaghib, A. Mauger, C. M. Julien, Olivine-Based Cathode Materials, Springer International Publishing Switzerland, 2015.
[6] S. Geller, J. L. Durand, Acta Crystallogr. **13**, 325 (1960).
[7] G. Križan, J. Križan, R. Dominko, M. Gaberšček, J. Power Sources **363**, 218 (2017).
[8] K. Ding, W. Li, Q. Wang, S. Wei, Z. Guo, J. Nanosci. Nanotechnol. **12**, 3812 (2012).
[9] K. S. Smirnov, V. A. Zhorin, N. A. Yashtulov, Russ. J. Appl. Chem. **86**, 603 (2013).
[10] S. Yang, P. Y. Zavalij, M. S. Whittingham, Electrochem. Commun. **3**, 505 (2001).
[11] R. Dominko, M. Bele, M. Gaberscek, M. Remskar, D. Hanzel, J. M. Goupil, S. Pejovnik, J. Jamnik, J. Power Sources **153**, 274 (2006).
[12] J. H. Lee, K. Y. Jung, S. B. Park, J. Mater. Sci. **34**, 4089 (1999).
[13] G. Arnold, J. Garche, R. Hemmer, S. Strobele, C. Vogler, M. Wohlfahrt-Mehrens, J. Power Sources **119-121**, 247 (2003).
[14] T. H. Cho, H. T. Chung, J. Power Sources **133**, 272 (2004).
[15] A. Varma, A. S. Mukasyan, A. S. Rogachev, K. V. Manukyan, Chem. Rev. **116**, 14493 (2016).
[16] X. Meng, W. de Jong, T. Kudra, Renew. Sustain. Energy Rev. **55**, 73 (2016).
[17] G. Križan, J. Križan, I. Bajsić, M. Gaberšček, Instrum. Sci. Technol. **46**, 43 (2018).
[18] G. Rousse, J. Rodriguez-Carvajal, S. Patoux, C. Masquelier, Chem. Mater. **15**, 4082 (2003).
[19] P. Gibot, M. Casas-Cabanas, L. Laffont-Dantras, S. Levasseur, P. Carlach, S. Hamelet, J.-M. Tarascon, C. Masquelier, Nat. Mater. **7**, 741 (2008).
[20] D. Jugović, M. Mitrić, M. Milović, B. Jokić, M. Vukomanović, D. Suvorov, D. Uskoković, Powder Technology **246**, 539 (2013).
[21] S. Shi, H. Zhang, X. Ke, C. Ouyang, M. Lei, L. Chen, Phys. Letters A **373**, 4096 (2009).
[22] C. M. Burba, R. Frech, Spectrochim. Acta A **65**, 44 (2006).
[23] C. M. Julien, K. Zaghib, A. Mauger, H. Groult, Advances in Chemical Engineering and Science **2**, 321 (2012).
[24] A. A. Salah, P. Jozwiak, J. Garbarczyk, K. Benkhouja, K. Zaghib, F. Gendron, C. M. Julien, J. Power Sources **140**, 370 (2005).
[25] A. Ait-Salah, J. Dodd, A. Mauger, R. Yazami, F. Gendron, C. M. Julien, Z. Anorg. Allg. Chem. **632**, 1598 (2006).
[26] W. Kang, C. Zhao, R. Liu, F. Xu, Q. Shen, Cryst. Eng. Comm. **14**, 2245 (2012).
[27] N. Ravet, M. Gauthier, K. Zaghib, J.B. Goodenough, A. Mauger, F. Gendron, C. M. Julien, Chem. Mater. **19**, 2595 (2007).
[28] V. Palomares, A. Goñi, A. Iturrondobeitia, L. Lezama, I. de Meatza, M. Bengoechea, T. Rojo, J. Mater. Chem. **22**, 4735 (2012).

*Corresponding author: lzorica@yahoo.com